General Synthesis of Periodic Macroporous Solids by Templated Salt Precipitation and Chemical Conversion

Hongwei Yan,[†,‡] Christopher F. Blanford,[†] Brian T. Holland,[†] William H. Smyrl,[‡] and Andreas Stein*[,†]

Department of Chemistry, University of Minnesota, Minneapolis, Minnesota 55455, and Department of Chemical Engineering and Materials Science, University of Minnesota, Minneapolis, Minnesota 55455

Received December 14, 1999. Revised Manuscript Received February 8, 2000

This paper presents a general method to prepare three-dimensionally ordered macroporous (3DOM) metal oxides or carbonates via templating with polystyrene (PS) spheres. The method is based on templated precipitation of metal salts (acetates, oxalates, oxides) within a colloidal crystal of PS spheres and subsequent chemical conversion of the inorganic precursors. The compositional range of possible macroporous products includes oxides or carbonates of many metals in the periodic table (e.g., MgO, Cr_2O_3, Mn_2O_3, Fe_2O_3, Co_3O_4, NiO, ZnO, $CaCO_3$), including compositions that are less accessible or more expensive by previous syntheses based on metal alkoxide precursors. Optimal synthesis conditions and structural features of selected materials are described, on the basis of XRD, TGA, SEM, TEM, nitrogen adsorption data, and chemical analysis.

Introduction

Macroporous (pores ≥ 50 nm) metal oxides have been used as filtration and separation materials,[1,2] catalyst supports,[3] carriers for cell immobilization,[4] battery materials,[5] and thermal insulators.[6] Conventional methods to prepare macroporous metal oxides involve mixing metal oxide particles with some type of binder. Because of nonuniform particle sizes, it is difficult to control the shape of pores; meanwhile, a broad pore size distribution and low porosity are usually obtained. Templating methods provide alternative preparations for macroporous solids. By using polymer gels,[7,8] emulsions,[9,10] latex spheres,[11] even bacteria[12] as templates, it is possible to prepare well-defined macroporous metal oxides with narrow macropore size distributions. Recently developed colloidal crystal templating techniques have permitted chemical preparations of macroporous materials with three-dimensionally ordered arrays of pores with diameters from tens to hundreds of nanometers.[13−28] These macroporous products are obtained by filling the spaces between a close-packed array of polystyrene or silica spheres with a precursor fluid which forms a solid skeleton around the spheres. Because the pore size is comparable to the wavelength of visible light, dielectric materials with three-dimensionally ordered macroporous (3DOM) structures are potential candidates for three-dimensional photonic crystals with optical band gaps.[17] These crystals are predicted to have useful optical properties, such as inhibition of spontaneous emission or photon localization, generating wide interest in applications including optoelectronics and optical com-

* Correspondence and requests for materials should be addressed to A.S. (e-mail: stein@chem.umn.edu).
[†] Department of Chemistry.
[‡] Department of Chemical Engineering and Materials Science.

(1) Sarrade, S. J.; Rios, G. M.; Carles, M. *Sep. Purif. Technol.* **1998**, *14*, 19−25.
(2) Nakanishi, K.; Minakuchi, H.; Soga, N.; Tanaka, N. *J. Sol-Gel Sci. Technol.* **1998**, *13*, 163−169.
(3) Diddams, P. *Inorganic Supports and Catalysts*; Smith, K., Ed.; Ellis Horwood: New York, 1992; pp 3−39.
(4) Aivasidis, A.; Wandrey, C.; Kiefer, W. U.S. Patent 5 096 814, 1992.
(5) Clough, T. J. U.S. Patent 5 895 732, 1999.
(6) Litovsky, E.; Shapiro, M.; Shavit, A. *J. Am. Ceram. Soc.* **1996**, *79*, 1366−1376.
(7) Yang, P.; Deng, T.; Zhao, D.; Feng, P.; Pine, D.; Chmelka, B. F.; Whitesides, G. M.; Stucky, G. D. *Science* **1998**, *282*, 2244−2246.
(8) Caruso, R. A.; Giersig, M.; Willig, F.; Antonietti, M. *Langmuir* **1998**, *14*, 6333−6336.
(9) Imhof, A.; Pine, D. J. *Nature* **1997**, *389*, 948−951.
(10) Imhof, A.; Pine, D. J. *Adv. Mater.* **1998**, *10*, 697−700.
(11) Antonietti, M.; Berton, B.; Göltner, C.; Hentze, H. P. *Adv. Mater.* **1998**, *10*, 154−159.
(12) Davis, S. A.; Burkett, S. L.; Mendelson, N. H.; Mann, S. *Nature* **1997**, *385*, 420−423.
(13) Velev, O. D.; Jede, T. A.; Lobo, R. F.; Lenhoff, A. M. *Nature* **1997**, *389*, 447−448.
(14) Velev, O. D.; Jede, T. A.; Lobo, R. F.; Lenhoff, A. M. *Chem. Mater.* **1998**, *10*, 3597−3602.
(15) Holland, B. T.; Blanford, C. F.; Stein, A. *Science* **1998**, *281*, 538−540.
(16) Holland, B. T.; Blanford, C. F.; Do, T.; Stein, A. *Chem. Mater.* **1999**, *11*, 795−805.
(17) Wijnhoven, J. E. G. J.; Vos, W. L. *Science* **1998**, *281*, 802−804.
(18) Zakhidov, A. A.; Baughman, R. H.; Iqbal, Z.; Cui, C.; Khayrullin, I.; Dantas, S. O.; Marti, J.; Ralchenko, V. G. *Science* **1998**, *282*, 897−901.
(19) Park, S. H.; Xia, Y. *Chem. Mater.* **1998**, *10*, 1745−1747.
(20) Park, S. H.; Xia, Y. *Adv. Mater.* **1998**, *10*, 1045−1048.
(21) Vlasov, Y. A.; Yao, N.; Norris, D. J. *Adv. Mater.* **1999**, *11*, 165−169.
(22) Johnson, S. A.; Ollivier, P. J.; Mallouk, T. E. *Science* **1999**, *283*, 963−965.
(23) Gates, B.; Yin, Y.; Xia, Y. *Chem. Mater.* **1999**, *11*, 2827−2836.
(24) Subramania, G.; Constant, K.; Biswas, R.; Sigalas, M. M.; Ho, K. M. *Appl. Phys. Lett.* **1999**, *74*, 3933−3935.
(25) Subramania, G.; Manoharan, V. N.; Thorne, J. D.; Pine, D. J. *Adv. Mater.* **1999**, *11*, 1261.
(26) Yan, H.; Blanford, C. F.; Holland, B. T.; Parent, M.; Smyrl, W. H.; Stein, A. *Adv. Mater.* **1999**, *11*, 1003−1006.
(27) Jiang, P.; Cizeron, J.; Bertone, J. F.; Colvin, V. L. *J. Am. Chem. Soc.* **1999**, *121*, 7957−7958.
(28) Velev, O. D.; Tessier, P. M.; Lenhoff, A. M.; Kaler, E. W. *Nature* **1999**, *401*, 548.

10.1021/cm9907763 CCC: $19.00 © 2000 American Chemical Society
Published on Web 03/17/2000

Table 1. Experimental Conditions for the Synthesis of 3DOM Metal Oxides

element	precursor	solvent	calcd *T*, °C	product	PDF file	applications[d]
Ni	$Ni(Ac)_2 \cdot 4H_2O$	10 mL of CH_3COOH[a]	360	NiO, bunsenite	04-0835	sensor, electrode
Co	$Co(Ac)_2 \cdot 4H_2O$	10 mL of CH_3COOH[a]	400	Co_3O_4	42-1467	sensor
Mn	$Mn(Ac)_2 \cdot 4H_2O$	10 mL of EtOH	450	Mn_2O_3, Bixbyite−C	41-1442	N/A
Mg	$Mg(Ac)_2 \cdot 4H_2O$	5 mL of EtOH/5 mL of H_2O	500	MgO, periclase	45-0946	catalyst support
Ca	$Ca(Ac)_2 \cdot H_2O$	3 mL of EtOH/7 mL of H_2O[a]	500	$CaCO_3$, calcite	05-0586	N/A
Zn	ZnO	10 mL of CH_3COOH/5 mL of H_2O	400	ZnO, zincite	36-1451	sensor
Fe	$FeC_2O_4 \cdot 2H_2O$	5 mL of EtOH/5 mL of H_2O/H_2O_2[b]	450	Fe_2O_3, hematite	33-0664	sensor
Cr	CrO_3	5 mL of EtOH/5 mL of H_2O[c]	450	Cr_2O_3, eskolaite	38-1479	N/A

[a] Undissolved solid removed by filtration. [b] Two grams of oxalic acid was added to the mixture of $FeC_2O_4 \cdot 2H_2O$ in water. A 30% aqueous H_2O_2 solution was added dropwise until all solids were dissolved. Fe(II) oxalate was oxidized to Fe(III) oxalate by this procedure. Ethanol was added at this stage. [c] Excess oxalic acid (6−8 g) was added to the mixture of CrO_3 in water. Ethanol was added after all solids had dissolved. [d] Actual applications of the bulk oxides are listed. These may be potential applications for the 3DOM metal oxides.

munications. At present, one of the main experimental challenges lies in the preparation of a large "single crystal" for optical applications, because it is difficult to obtain large, single-phase colloidal crystals as templates and to remove the templates in a controlled way without disrupting the structure of the inorganic skeleton. On the other hand, relatively straightforward preparations are currently available for multiphase colloidal crystals composed of smaller ordered domains in various orientations. Another requirement for photonic crystals and certain other applications is the ability to vary the dielectric constant of the walls by controlling the wall composition. To gain better insight into structural control, it is necessary to investigate the synthesis−structure−property relationships of 3DOM metal oxides.

Although several routes have been reported to prepare 3DOM structures by colloidal crystal templating methods, 3DOM metal oxides (oxides of Si, Ti, Zr, Al, Sb, W, Fe, and mixtures of some of these) have only been synthesized by alkoxide-based sol−gel processes.[13−17,29,30] In these processes, liquid metal alkoxides, either neat or in solution, were first introduced into the spaces between the templating sphere array; subsequently a solid metal oxide skeleton was constructed via in situ sol−gel transformation, which maintained its shape after the templating agents were removed. However, this method is most suitable for the preparation of high-valence metal oxides. For many low-valence transition metal oxides and alkaline earth metal oxides, the formation of an ordered 3D framework becomes more difficult, if the alkoxide precursors hydrolyze/polymerize too rapidly to fill the voids in the template, or if they have a low solubility in a solvent that is compatible with the template array. Moreover, the high cost and difficulty of obtaining certain metal alkoxide precursors commercially hinder research progress in the fabrication of these important functional materials with 3DOM structures.

Regardless of the precursor, the template material, and the template packing or removal methods, the key point of the colloidal crystal templating method lies in the design of a fluid−solid transformation which takes place in the interstices of the colloid crystals. For example, Zakhidov et al. prepared glassy carbon, graphitic carbon, or diamond by a phenolic route, chemical vapor deposition (CVD), or plasma-enhanced CVD method;[18] Park et al. used UV-curable or thermally curable precursor methods to synthesize polymers;[19] Vlasov et al. introduced presynthesized nanocrystals inside the silica spheres templates to prepare CdSe;[21] and Jiang et al. applied an electroless deposition technique to prepare macroporous metal films.[27] This paper describes a new fluid−solid transformation as a general method to prepare 3DOM structures involving low-valent metal salts. The method is based on templated precipitation and subsequent chemical conversion of the precursors. The compositional range of the possible macroporous products includes oxides (or carbonates) of most metals in the periodic table. This paper provides examples for the preparation of oxides of Mg, Cr, Mn, Fe, Co, Ni, Zn, as well as $CaCO_3$ to illustrate the general applicability of this facile templating method. Optimal synthesis conditions and structural features of these materials are described, based on X-ray diffraction (XRD), TGA, scanning electron microscopy (SEM), transmission electron microscopy (TEM), nitrogen adsorption data, and chemical analysis.

Experimental Section

Materials. Monodisperse polystyrene (PS) spheres were synthesized and packed into colloidal crystals by centrifugation as described previously.[16] Sphere diameters in various batches ranged from 620 ± 10 nm to 760 ± 25 nm. Manganese(II) acetate tetrahydrate (99%), cobalt(II) acetate tetrahydrate (98%), nickel(II) acetate tetrahydrate (98%), zinc oxide (99%), magnesium acetate tetrahydrate (99%), calcium acetate monohydrate (99%), chromium(VI) oxide (99%), iron(II) oxalate dihydrate (99%), and oxalic acid (98%) were obtained from Aldrich. All the precursors were used as received without further purification.

Synthesis of 3DOM Metal Oxides or Carbonate. A metal acetate or another appropriate precursor salt (2 g) was dissolved in the amount of solvent or solvent mixture listed in Table 1. Centimeter-scale, close-packed, colloidal polystyrene crystals (∼2 g) were soaked in this solution for 3−5 min. Excess solution was removed from the impregnated colloidal crystals by vacuum filtration. The samples were dried at 65 °C for 1 h. The dried composites were soaked in 10 mL of oxalic acid solution (∼30 g oxalic acid in 100 mL of ethanol) for 5−10 min. Certain precursors, such as iron(III) oxalate and chromium(III) oxalate, which were soluble in water, could be used directly without the second precipitation step involving oxalic acid. For the Ca, Mg, and Zn samples, the composites were annealed at 110−120 °C for 5−15 min before being soaked in the oxalic acid solution. After an additional vacuum filtration and drying step, the polystyrene spheres were removed by heating first in fast-flowing air (1.0 L/min in a 22 mm i.d. quartz tube) at 300 °C for 5 h, and then calcining for 10 h in slow-flowing air (0.1 L/min) at the calcination temperature listed in Table 1. All the heating rates were 1 °C/min.

(29) Blanford, C. F.; Do, T. N.; Holland, B. T.; Stein, A. *Mater. Res. Soc. Symp. Proc.*; Lednor, P. W., Nagaki, D. A., Thompson, L. T., Eds.; MRS: Warrendale, PA, 1999; Vol. 549, pp 61−66.

(30) Holland, B. T.; Abrams, L.; Stein, A. *J. Am. Chem. Soc.* **1999**, *121*, 1, 4308−4309.

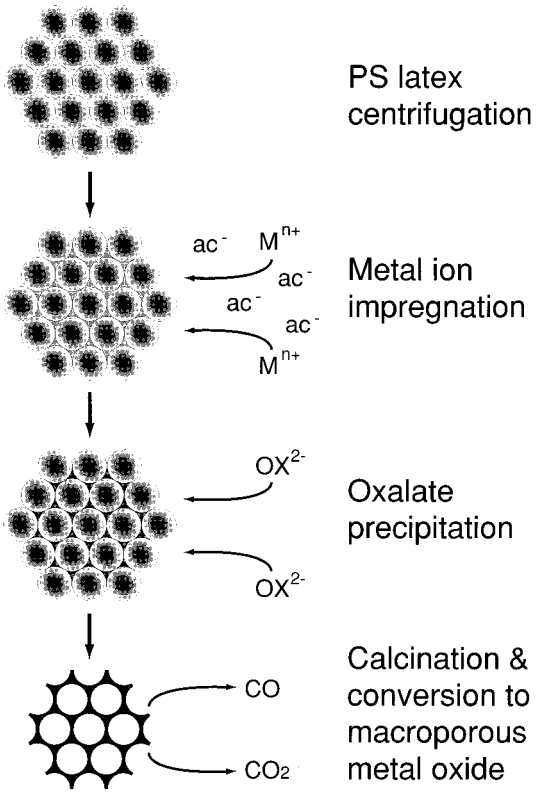

Figure 1. Schematic diagram of the templated precipitation/chemical conversion method used to fabricate 3DOM metal oxides.

Characterization. Powder X-ray diffraction (XRD) studies were performed on a Siemens D5005 wide-angle XRD spectrometer with Cu Kα radiation. Average grain-size determinations were based on fitting the XRD patterns by using the JADE5 program. Thermogravimetric analysis (TGA) was performed with a Perkin-Elmer TGA-7 thermogravimetric analyzer attached to a PC via a TAC7/DX thermal controller. Differential scanning calorimetry (DSC) was carried out with a Perkin-Elmer 7 differential scanning calorimeter. A Hitachi S-800 scanning electron microscope (SEM) was used to examine the morphology of the samples. The $CaCO_3$, MgO, and ZnO samples, which are insulators with wide band gaps, were coated with 5-nm Pt to reduce surface charging. The other semiconducting materials were not metal coated for SEM; no deleterious charging effects were observed. Transmission electron micrographs (TEM) were recorded on film with a Philips CM30 TEM operating at 300 kV with a LaB_6 filament. Samples for TEM were prepared by sonicating about 20 mg of the powder in 2 mL of absolute ethanol for 30 min, and then depositing five drops of the suspension on a holey carbon grid. Micrographs were scanned on a Microtek ScanMaker III scanner for further analysis. Chemical analyses for carbon and hydrogen were carried out at Atlantic Microlab, Inc., Norcross, GA. Nitrogen adsorption measurements were performed on a Micromeritics ASAP 2000 sorption analyzer. Prior to the sorption measurements, the samples were degassed under vacuum at 120 °C until a pressure ≤3 μmHg was obtained. Surface areas were calculated by the Brunauer−Emmett−Teller (BET) method; pore volumes and pore size distributions were determined from the adsorption isotherms by the Barrett−Joyner−Halenda (BJH) method. Mercury porosimetry measurements were carried out on a Micromeritics Poresizer 9320.

Results and Discussion

Preparation of the Latex-Templated Precursor. Figure 1 illustrates the preparation of the 3DOM metal oxides by the precipitation/chemical conversion method. To obtain well-ordered macroporous products by the colloidal crystal templating method, several requirements should be satisfied by both the solvent and the precursor. First, the solvent should wet the polystyrene spheres well so that the fluid can penetrate the template array completely and to eliminate faults in the final structure produced by nonwetted regions. Second, the precursor should have a high solubility in the solvent to maximize the precursor loading and produce strong enough walls in the calcined solid to avoid collapse. Third, the precursor should not melt at a temperature where the latex softens (to avoid phase separation); or it should have a melting point higher than the temperature at which the latex spheres are gasified and burnt.

In this work, ethanol and acetic acid were used as suitable solvents to achieve good wetting of the closely packed polystyrene spheres, as were their mixtures with water, although water by itself did not wet the polystyrene spheres. Alternatively, one could also change the surface functionality of the polymer spheres to improve wetability in an optimal solvent. The metal salt solution penetrated the void spaces within the latex sphere array by capillary forces, depositing the metal salt inside the array after solvent removal. As candidates for precursor metal salts, either acetates or nitrates of the metals used here had an acceptable solubility in the chosen solvents. However, they did not meet the third requirement because of their low melting points. In our experiments, heating the metal acetate/PS composites resulted in their completely melting so that no more ordered structure remained. It is well-known that many metal oxalates decompose directly before melting, but most of them are insoluble in water, ethanol, or acetic acid. To combine the advantages of the two kinds of salts above, we designed an in situ chemical reaction by inducing oxalic acid solution into the metal acetate or nitrate-soaked PS array and transforming the low-melting, soluble salts to nonmelting salts. Because of the relative strengths of their conjugate acids compared to oxalic acid, acetates are the preferred precursors over nitrates. A few soluble oxalates, such as iron(III) oxalate and chromium(III) oxalate, can be used directly as precursors since they already meet the requirements. It should be noted that the timing for the precipitation reaction is critical to obtain 3DOM oxides of Mg, Ca, and Zn. If the composites of acetates/PS are immersed in the oxalic acid solution too long, swelling can cause a breakup of the latex sphere array and lead to lower macropore periodicity. To avoid this problem, the composites can be heated at 110−120 °C for 5−15 min. This annealing treatment results in partial fusing of the PS spheres and endows the colloidal crystal with enough strength to withstand breakup, while preserving open channels for the incorporation of oxalic acid.

Compared with methods involving sol−gel precursors, this synthetic procedure is less sensitive to atmospheric humidity. The precursors used here are typically much less expensive than alkoxide precursors. The method also permits formation of ordered structures for compositions that might be difficult to prepare by sol−gel methods if the corresponding alkoxide precursors have low solubility, or if commercial alkoxide precursors are not readily available. Since a large number of fluid−solid transformation reactions can be designed to meet

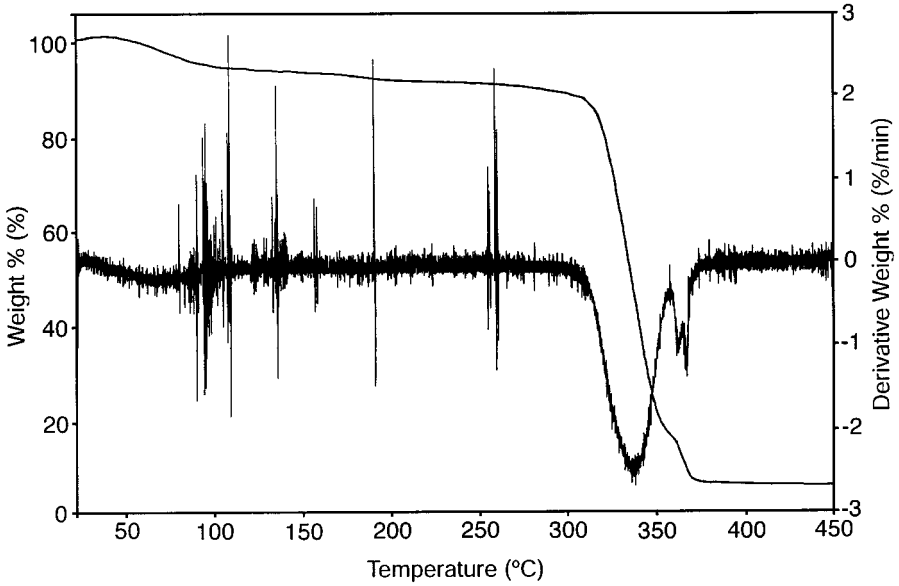

Figure 2. TGA and derivative TGA curves of a PS/nickel oxalate composite in a flowing air atmosphere. The sample was heated from 25 to 450 °C at 1.0 °C/min.

the requirements, the varieties of 3DOM metal oxides can be expanded extensively, covering most metals in the periodic table.

Calcination of Latex Templates and Subsequent Chemical Conversion. The latex templates were removed by calcination. It was found that the calcination conditions have an important effect on the quality of the macroporous product. During calcination, polystyrene undergoes several processes, such as glass transition, decomposition, and oxidation. The temperature ranges for these physical/chemical changes can be determined by DSC and TGA methods. On the basis of DSC measurements, the glass transition temperature for the polystyrene beads used as templates ranged from 93 to 108 °C. The decomposition and oxidation temperatures are influenced by the heating history, such as heating rate and airflow. Figure 2 shows the TGA curve for a PS/nickel oxalate composite calcined under flowing air from room temperature to 450 °C at a rate of 1 °C/min. The weight decrease below 100 °C is assigned to loss of residual solvent. A slow and steady weight loss from 100 to 310 °C is attributed to dehydration of $NiC_2O_4 \cdot 2H_2O$. Above 310 °C, the weight loss accelerates due to combustion of the polystyrene, a highly exothermic process that can be detrimental to the product structure if excessive bubbling results from the gas production. Thus, the removal of polystyrene should be performed at a temperature where weight loss occurs gradually; 300 °C was used in this work. The heating rate and airflow also have an effect on the removal of polystyrene, and need to be balanced. Slower heating rates (e.g., 2 °C/min) facilitate more even melting and decomposition of polystyrene, thus avoiding excessive bubbling, which is observed at faster rates (e.g., 10 °C/min). On the other hand, fast airflow aids the transport of byproducts and accelerates the decomposition reaction. For example, in the preparation of 3DOM NiO, it takes 3 h to remove most polystyrene at 300 °C with an airflow of 1.0 L/min in a tube oven with an inner diameter of 22 mm. However, it takes more than 20 h when the rate of airflow is 0.1 L/min.

Concomitant with or after the removal of latex spheres, the metal oxalates undergo decomposition and oxidation reactions. It can be seen in Figure 2 that a second set of weight loss peaks occurs at 360−370 °C, which are more apparent in the derivative curve. These peaks are attributed to the decomposition of nickel oxalate to nickel with subsequent oxidation to nickel oxide. Nagase et al. and others investigated the temperatures and products of thermal decomposition of bivalent metal oxalates in nitrogen.[31−34] Depending on the radii of metal ions, the oxalates decomposed to metal carbonates, metal oxides, or metals at temperatures ranging from 235 to 418 °C. The decomposition reactions of various oxalates were described as follows:

$$MC_2O_4 \rightarrow MCO_3 + CO$$

where M = Ca(II), Sr(II), and Ba(II),

$$MC_2O_4 \rightarrow MO + CO + CO_2$$

where M = Mg(II), Mn(II), Fe(II), Zn(II), and Sn(II), and

$$MC_2O_4 \rightarrow M + CO_2$$

where M = Co(II), Ni(II), Cu(II), Cd(II), and Pb(II).

In an air atmosphere, Cu, Cd, Pb, and Ni were oxidized further.[33,35]

In the present work, we investigated the products of oxalates of Mn(II), Co(II), Ni(II), Zn(II), Mg(II), Ca(II), Fe(III), and Cr(III) after calcination at temperatures ranging from 360 to 450 °C for 1−10 h. Carbon (0.1−0.4 wt %) and hydrogen (0−0.3%) analyses of these products indicated that the PS templates were nearly completely removed during calcination and that the oxalate precursors had been fully decomposed. Powder

(31) Nagase, K.; Sato, K.; Tanaka, N. *Bull. Chem. Soc. Jpn.* **1975**, *48*, 439−442.
(32) Mansour, S. A. A. *Thermochim. Acta* **1993**, *230*, 243−257.
(33) Dollimore, D.; Griffiths, D. L.; Nicholson, D. *J. Chem. Soc.* **1963**, 2617−2623.
(34) Robin, J. *Bull. Soc. Chim. France* **1953**, 1078−1084.
(35) Yong, W. J.; Hall, B. *Thermochim. Acta* **1989**, *147*, 251−260.

Table 2. Microstructure, Surface Areas, and Porosity Data for 3DOM Metal Oxides

sample composition	grain size[a] (nm)	BET surface area (m^2/g)	pore volume[b] (mL/g)	pore diameter[c] (nm)	macropore diameter[d] (nm)	PS sphere diameter[d] (nm)	wall thickness[d] (nm)
NiO	10 ± 1	63	0.21	13	470 ± 10	660 ± 15	60 ± 10
Co_3O_4	35 ± 6	25	0.13	26	500 ± 20	640 ± 25	55 ± 10
Mn_2O_3	35 ± 3	20	0.10	21	380 ± 20	660 ± 15	70 ± 15
MgO	7 ± 1	35	0.19	26	455 ± 15	640 ± 10	60 ± 20
$CaCO_3$	41 ± 8	13	0.03	14	560 ± 40	760 ± 25	140 ± 20
ZnO	21 ± 1	24	0.12	18	450 ± 15	760 ± 25	50 ± 15
Fe_2O_3	23 ± 1	39	0.18	18	550 ± 20	760 ± 25	60 ± 10
Cr_2O_3	30 ± 3	42	0.12	10	465 ± 15	760 ± 25	45 ± 15

[a] Grain sizes were calculated from XRD data. [b] Average BJH pore volumes from the adsorption pore volume plots. [c] Average BJH pore diameters from the adsorption pore volume plots. [d] Macropore diameters, PS sphere diameters, and wall thicknesses were estimated from SEM images.

XRD studies showed that all samples were crystalline and could be identified as the single phases listed in Table 1. Grain-size analyses based on the full width at half-maximum (fwhm) of diagnostic XRD reflections showed that the oxides were composed of nanoscale grains with sizes ranging from 7 to 41 nm (Table 2). For the oxalates of Mn(II), Co(II), Ni(II), and Fe(II), the phases Mn_2O_3, Co_3O_4, NiO, and Fe_2O_3 were obtained rather than lower oxidation-state products, because these oxalates were calcined in air, and any low oxidation-state decomposition products could be further oxidized in an exothermic reaction.[33,35] Fast airflow tended to accelerate combustion of the samples and often destroyed the ordered structures. Therefore, slow airflow was preferred during the final decomposition stage of oxalates.

The as-prepared 3DOM metal oxides (or carbonates) can be posttreated in different atmospheres to derive other 3DOM materials. For example, 3DOM metal nickel was obtained by reducing 3DOM NiO in a H_2 flow at 300 °C for 2 h.[26] It is also possible to prepare 3DOM calcium phosphate by treating 3DOM $CaCO_3$ with phosphoric acid.[36] This versatility of calcination conditions and posttreatment will undoubtedly facilitate the preparation of novel 3DOM materials, providing a broad basis to study their structure−property relationships.

Characterization of the Inorganic 3DOM Structures. Figure 3(a−h) shows the scanning electron microscopy (SEM) images of 3DOM structures composed of NiO, Co_3O_4, Mn_2O_3, Fe_2O_3, Cr_2O_3, ZnO, MgO, and $CaCO_3$. Although the microscopic morphology differs between samples, it can be seen that the close packing order of the original PS sphere template is preserved in all calcined products. NiO and Co_3O_4 formed the most regular structures. Well-ordered air spheres and interconnected inorganic walls create a "honeycomb" pore structure in three dimensions. Although the structure is sometimes partially obscured by fragments and fractures on the surface, the next several layers are still visible in the images. Because the latex templates were fabricated by centrifugation resulting in polycrystalline colloidal crystals, the structures are subdivided into many ordered domains of macropore arrays. The macropore units are often repeated for tens to hundreds of times without faults. Most of these domains have the typical fcc structure. Different views of the air sphere arrays can be classified as corresponding to planes of the fcc structure, such as {111} or {011}.[16] Given an ideal, single-phase colloidal crystal as template, one would expect that a perfect 3DOM structure can be prepared by this method under optimized conditions.

Besides originating from the template, defects may also arise from the synthesis procedure, depending on the material's composition and heating history. For example, the Mn_2O_3 structure (Figure 3c) appears to undulate, containing many fault planes and cracks. We believe that these defects are caused by the rapid production of CO_2 and CO during decomposition of manganese(II) oxalate, followed by exothermic oxidation of the CO. In the case of $CaCO_3$ (Figure 3e), the walls of the macropores are thicker than those of the other metal oxides (see Table 2), due to the higher minimum calcination temperature (500 °C) required to obtain the carbonate by our method and the rapid growth of grains at this temperature. For Fe_2O_3 (Figure 3g), the structural order is superior to that of a similar material prepared by the sol−gel method, since Fe_2O_3 tends to form larger wall crystallites and, hence, less ordered macroporous products when prepared from the alkoxide precursors.[29]

The open nature of the structure was confirmed by mercury porosimetry, using macroporous nickel oxide as an example. A total intrusion volume of 1.1 mL/g was measured for pores > ∼70 nm. Smaller pores, which require higher mercury pressures, could not be determined for this sample due to the fragile nature of the intricate metal oxide skeleton. From the measured bulk density of 0.57 g/mL, a porosity of ≥91% was calculated for macroporous nickel oxide. TGA measurements were employed as an alternate method to estimate the fraction of NiO left after calcination as compared to the maximum possible if all available interstitial space between close packed spheres (∼26 vol %) was filled with the $NiC_2O_4 \cdot 2H_2O$ precursor. With complete filling, the mass fraction of $NiC_2O_4 \cdot 2H_2O$ in the composite with PS spheres would be 44.9% (or 18.4% NiO), assuming densities of 1.05 g/cm^3 for PS and 2.44 g/cm^3 for $NiC_2O_4 \cdot 2H_2O$. After correction for residual solvent, the NiO content determined by TGA was 7.1%, i.e., 0.39 of the theoretical maximum. Because of the higher density of NiO (6.67 g/cm^3) compared to the oxalate precursor, the final NiO framework occupied significantly less than the maximum interstitial volume.

The periodic spacing of the dielectric material making up the walls gives 3DOM materials a colored, opalescent appearance due to Bragg diffraction of visible light. Figure 4 shows bright-field optical micrographs of samples of MgO and NiO. The macroporous solids appear shiny and colored, even though bulk MgO is

(36) Melde, B. J.; Stein, A. Unpublished work.

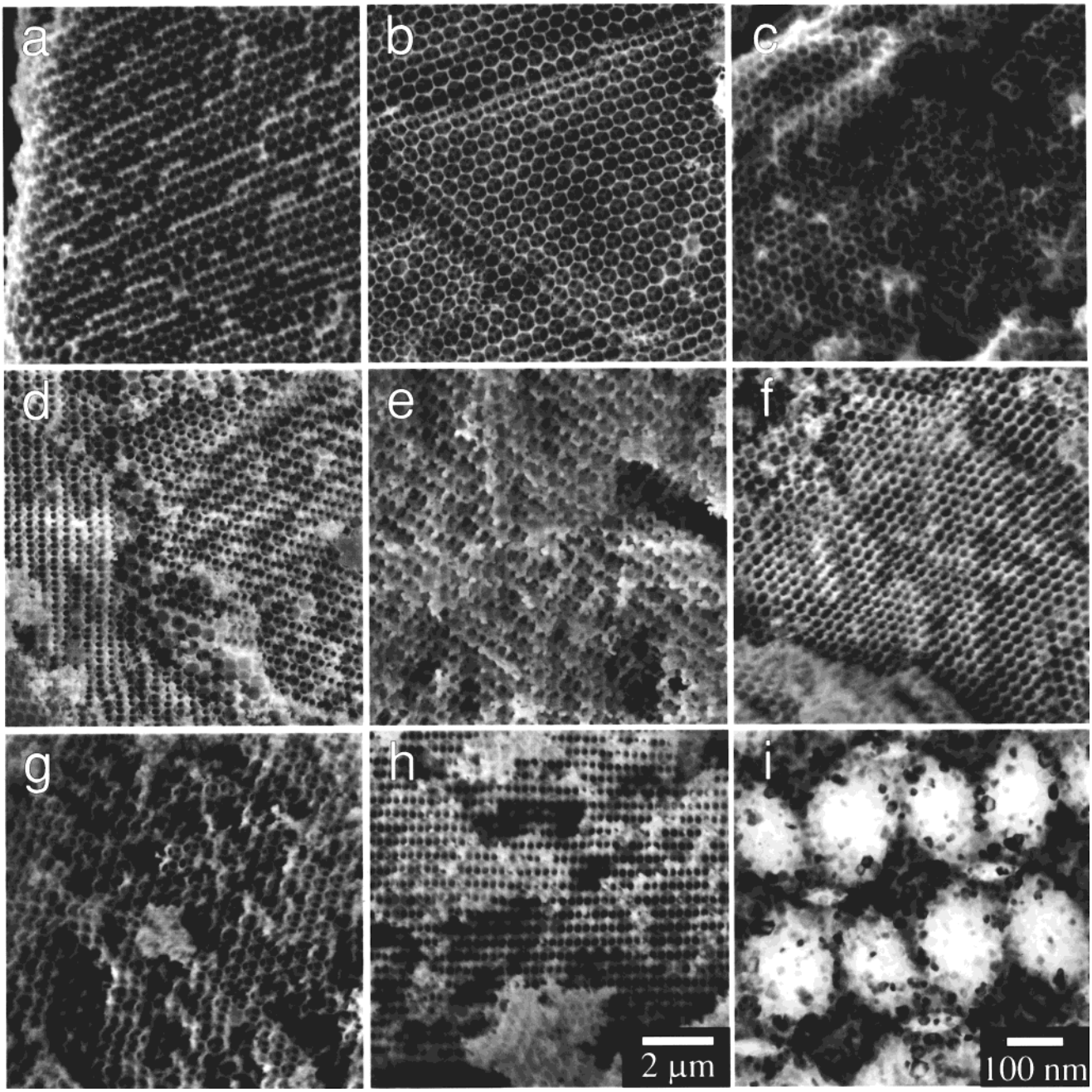

Figure 3. SEM images of 3DOM metal oxides: (a) NiO, (b) Co_3O_4, (c) Mn_2O_3, (d) MgO, (e) $CaCO_3$, (f) ZnO, (g) Fe_2O_3, and (h) Cr_2O_3. The scale is the same on all SEM images. Panel i is a TEM image of the wall structure of 3DOM NiO synthesized at 360 °C for 10 h.

white and bulk NiO is greenish-black. Similar opalescence is observed in other 3DOM samples.

The pore sizes and wall thicknesses of these samples (Table 2) were estimated from SEM images, averaging a large number of data points. The macropores in these samples are relatively monodisperse and the pore diameters range from 380 to 560 nm, depending on the diameter of the templating PS spheres. All pore diameters are considerably smaller than the original latex spheres due to shrinkage during calcination. Differences in shrinkage can be attributed to different concentrations of precursors, synthetic conditions, and crystallization kinetics. Another noticeable aspect is the wall structure of the samples. The SEM results show that the wall thicknesses in these samples range from 45 to 140 nm, resulting from walls formed by nanoscale grains. Figure 3i shows a TEM image of the wall structure of 3DOM NiO. The walls are composed of fused grains with an average diameter of 10−15 nm, in agreement with the XRD results.

The wall structures were also characterized by nitrogen adsorption measurements. A type II nitrogen adsorption was observed for all the samples. To take an example, Figure 5 shows a typical isotherm plot for 3DOM NiO. The low-pressure portion of the almost linear middle section of the isotherm, which is attributed to unrestricted monolayer−multilayer adsorption, suggests that the sample is a nonporous or macroporous adsorbent. However, the hysteresis loop over a range of high P/P^0, which is associated with capillary condensation taking place in mesopores, indicates that textural mesopores exist within the wall

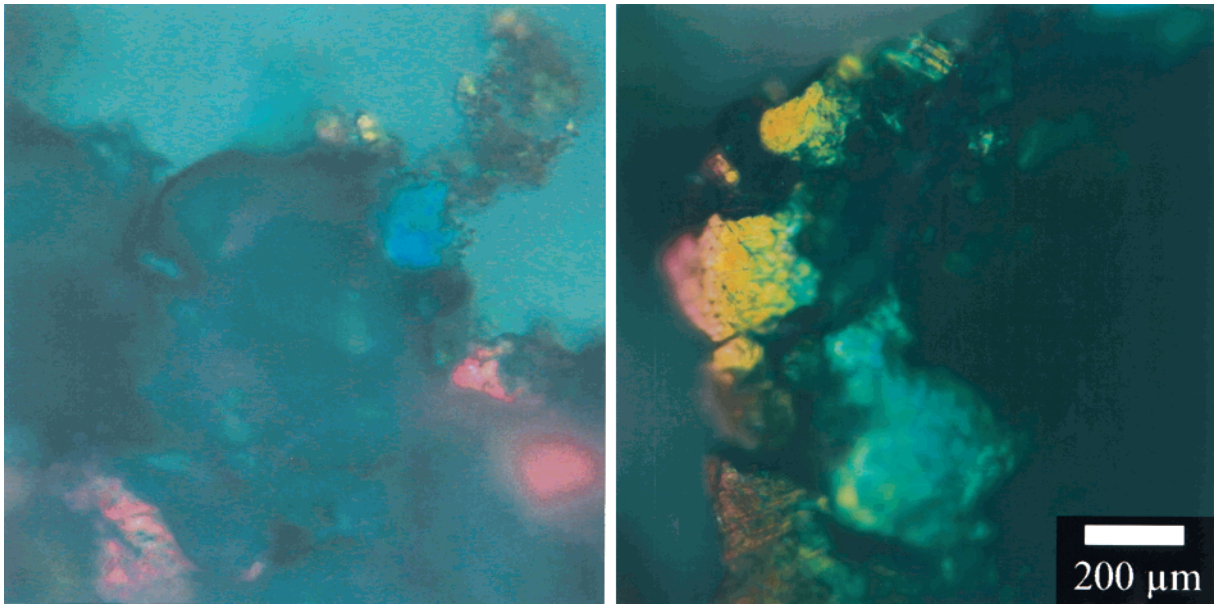

Figure 4. Bright field light microscope images of 3DOM: (a, left) MgO and (b. right) NiO.

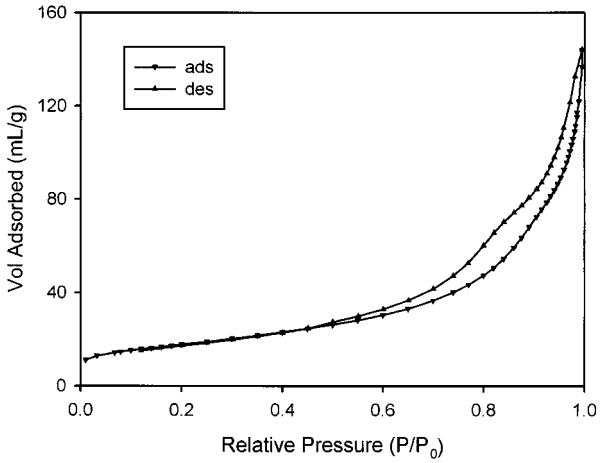

Figure 5. Nitrogen adsorption isotherm of 3DOM NiO synthesized at 360 °C for 10 h.

structure. Associated with TEM results, these data suggest that a loose aggregation of nanoscale grains forms the matrix of the wall structure and produces the mesoporosity. The average BJH pore diameter and the BET surface areas of each sample were calculated and are listed in Table 2. The average BJH pore diameter of these mesopores is about 10.5−25.6 nm, giving rise to BET surface areas between 12.8 and 63.1 m^2/g, depending on the material and calcination conditions. Therefore, these 3DOM materials possess a microstructure with dual porosity due to textural mesopores and larger, open macropores. The higher surface areas due to the mesopores are expected to influence interfacial processes.

The Effect of Synthesis Conditions on 3DOM Structures. In many applications 3DOM structures with specific pore sizes are required. One obvious way of adjusting pore sizes is to select latex spheres with appropriate sizes, taking into account shrinkage. In addition, one can tailor pore sizes by controlling synthesis conditions. To investigate the effect of the calcination temperature, 3DOM NiO was synthesized at different temperatures for 10 h. Figure 6 shows the SEM

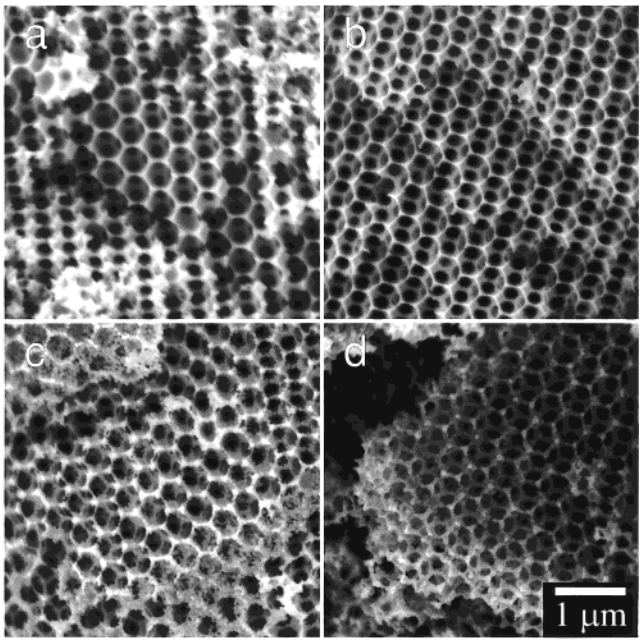

Figure 6. SEM images of 3DOM NiO synthesized at different temperatures for 10 h: (a) 360 °C, (b) 450 °C, (c) 550 °C, (d) 600 °C.

images of some selected samples. From 360 to 500 °C, the pore size remains virtually unchanged. When the temperature exceeds 500 °C, the pore size tends to decrease. This result suggests that two kinds of shrinkage occur during the calcination: one is due to shrinkage of the latex template, which appears to be independent of temperature; the other is attributed to the shrinkage of the wall structure as grains grow, which can be adjusted by varying the temperature and heating time. Figure 7 summarizes the dependence of pore size and grain size on the calcination temperature. The average grain size, based on powder XRD measurements, increases with temperature. As the grains become progressively larger, the apparent density of the wall tends to increase, causing a small amount of shrinkage of the macropores. At 550 °C individual grains are observed in the wall structure (Figure 6c).

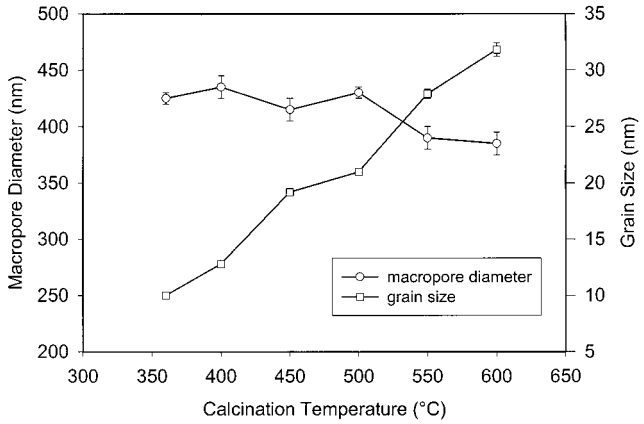

Figure 7. Variation of the pore diameters and grain sizes of 3DOM NiO as a function of calcination temperature. The diameter of the templating PS spheres was 620 ± 10 nm.

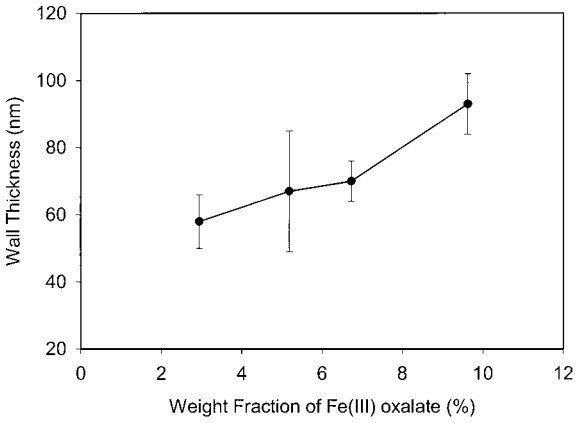

Figure 8. Variation of the wall thickness of 3DOM Fe_2O_3 as a function of precursor (iron(III) oxalate) loading. All the samples were synthesized at 450 °C for 1 h. Loading amounts were determined by TGA measurements. Weight fraction of iron(III) oxalate = (mass iron(III) oxalate)/(mass PS + mass iron(III) oxalate). Average wall thicknesses were estimated from SEM images on the basis of multiple measurements.

At 600 °C evidence for sintering is observed, resulting in growth of the nodal points and roughening of the connecting bridges (Figure 6d). With further sintering, the wall structure can collapse completely. The calcination time has a similar effect on the 3DOM structure as the temperature. By shortening the calcination time from 10 to 1 h, the average grain size of 3DOM NiO synthesized at 600 °C is reduced from 35 to 20 nm, and the wall surface still looks smooth. Therefore, by carefully controlling the growth of grains, a refinement of the pore size can be achieved.

The effect of the precursor concentration on 3DOM structures was also investigated. In this work, it was found that a minimal concentration of 0.5 M was necessary to fabricate a 3DOM structure. At lower concentrations, the solid skeleton did not have enough strength to support itself and collapsed during the removal of polystyrene. On the other hand, much higher concentrations of certain precursors made the solution too viscous to penetrate the latex array thoroughly. To increase the precursor loading, it is also possible to fill the template array multiple times with solutions at low concentrations.[17] Within the working range of concentrations, an increase in wall thickness was observed in a series of samples prepared with higher loadings of iron(III) oxalate, as shown in Figure 8. A similar trend was seen in multiple self-consistent series. Thus, by controlling the synthesis conditions, it is possible to modify wall thicknesses and thereby the size of openings between adjacent voids.

Conclusions

A general method was presented to fabricate 3DOM metal oxides or carbonates based on templated precipitation and subsequent chemical conversion. Because it is based on readily available inorganic salts as precursors, the synthetic procedure is less sensitive to the atmosphere and less expensive, compared with sol−gel processes. The versatility of this synthetic procedure combined with various posttreatments[26] can greatly expand the varieties of 3DOM compositions, which may now cover oxides (carbonates) of most metals in the periodic table. By controlling synthesis conditions, it is possible to tailor pore sizes and wall thicknesses according to specific requirements. These novel 3DOM dielectric or semiconducting materials have potential technological applications as catalysts, supports, sensors, waveguides, and porous electrodes or electrolytes.

Acknowledgment. We thank 3M, Dupont, the David and Lucille Packard Foundation, the McKnight Foundation, the National Science Foundation (DMR-9701507 and the MRSEC Program of the NSF under Award DMR-9809364), and the Department of Energy (DOE/DE-FG02-93-ER14384) for support of this research.

CM9907763